Article:
Nguyen, V.T.T., Ulamec, S.M., Brockwell, D. et al. (Accepted: 2026) In silico peptide self-assembly reveals the importance of N-terminal motifs and the inhibition mechanism of the mutation L38M in α-synuclein fibrillation. Protein Science. ISSN: 0961-8368 (In Press)

In silico peptide self-assembly reveals the importance of N-terminal motifs and the inhibition mechanism of the mutation L38M in α-synuclein fibrillation

Van T. T. Nguyen[1] | Sabine M. Ulamec[2] | David J. Brockwell[2] | Sheena E. Radford[2] | Carol K. Hall[1]

[1]Department of Chemical and Biomolecular Engineering, North Carolina State University, Raleigh, North Carolina, USA

[2]Astbury Centre for Structural Molecular Biology, School of Molecular and Cellular Biology, Faculty of Biological Sciences, University of Leeds, Leeds LS2 9JT, UK.

*Corresponding Author

Email: hall@ncsu.edu

ABSTRACT

Alpha-synuclein (αSyn) is a presynaptic protein associated with several neurodegenerative diseases. While the non-amyloid component (NAC) region of the αSyn sequence (residues 65-90) forms the core of all αSyn fibrils, recent findings suggest that the flanking regions play a key role in initiating or preventing amyloid formation. Two motifs in the N-terminal region, named P1 (αSyn[36-42]) and P2 (αSyn[45-57]), have been shown to be key modulators of fibril formation, with deletion of these regions, or single-point mutations in the P1 region inhibiting amyloid formation of full-length αSyn. In this study, we use the coarse-grained molecular dynamics package DMD/PRIME20 to simulate the self-assembly of the P1 and P2 regions, alongside longer segments P3 (αSyn[36-57]) and P3Next (αSyn[27-57]), and single-point mutations: focusing primarily on L38M, L38A, and V40A, and additionally examining Y39A and S42A as secondary variants, all of which have different effects on fibril formation of the full length protein *in vitro*. The results show that P1, P2 and P3 have a high propensity to form parallel β-sheets while P3Next tends to form β-hairpins within fibrillar structures. The L38M substitution reduces the formation of both parallel β-sheets and β-hairpins, consistent with the inability of full-length αSyn containing L38M to form amyloid fibrils *in vitro* at neutral pH and to aggregate *in vivo* in *C. elegans*. In contrast, simulations of L38A and V40A show no such effect, consistent with their minimal impact on full-length αSyn fibrillation. The simulation results suggest that the presence of P1/P2 hairpins are required to unleash the amyloid potential of αSyn and offer a structural explanation of how L38M mutation in this region protects the protein from amyloid formation.

KEYWORDS

α-synuclein, peptide self-assembly, amyloid fibril formation, DMD/PRIME20 simulations, N-terminal motifs/segments/fragments, mutation inhibitor, inhibitory mechanism, inter-domain interactions, β-hairpins, parallel β-sheets

ABBREVIATIONS

αSyn, α-Synuclein; DMD, discontinuous molecular dynamics.

LIST OF FIGURE LEGENDS

Figure 1 αSyn regions and the peptide fragments that were simulated herein. The amphipathic N-terminal (green) contains residues **αSyn[1-60]**. The central non-amyloid component (NAC) region (red) contains residues **αSyn[61-95]**. The acidic C-terminal region (orange) covers the last 45 residues. P1 and P2 are short motifs in the N-terminal region (light green). The sequences of P1, P2, P3, P3Next, and C1ext are listed. Note the charges on the termini are blocked in the simulation (see Methods).

Figure 2 Snapshots at different times during the early stage of fibril formation of P1-WT fragments from one simulation. See **also Supplementary Movie 1**.

Figure 3 (a) Simulation snapshot of final conformation and schematic representation of U-shaped and S-shaped conformation of P2 fibrils. Red indicates G51 and green shows all other residues. (b) Simulation snapshots of P3 fragments at the end of each run show mixed fibrils with different percentage of parallel residues within the fibrils. As P3 contains both P1 and P2, the color code is used to display the position of P1 (red), P2 (green), and the in-between residues αSyn[43-44] (blue). (c) Total interaction energy vs time for the four runs of P3-WT.

Figure 4 Conformational variability and β-hairpin statistics of P3Next-WT across seven independent simulations. (a) Snapshots at the ends of the simulations of P3Next-WT fragments reveal that the number of β-hairpins varies in the P3Next-WT fibrils. A color code is used to display the position of P1 (red), P2 (green), the in-between residues αSyn[43-44] (blue), and the additional residues in P3Next compared to P3 (orange). Enlarged section from the snapshot of Run 7 shows β-hairpins in the fibril. (b) Distribution of β-hairpin content for each of the seven independent P3Next-WT trajectories, shown as violin plots. Each violin displays the full probability density of β-hairpin counts during a run, with horizontal bars marking the mean and

vertical lines indicating extrema. (c) Pooled histogram of β-hairpin content across all frames from all seven WT trajectories shows that distribution is centered around 3–5 β-hairpins.

Figure 5 (a) Snapshots of final configurations of P1 peptide simulations with the sequence substitutions L38M, L38A or V40A, as well as the wild-type P1 (P1-WT). Although all four sequences formed multi-layer fibrils, the number of parallel and antiparallel β-strands are different. Each fibril is shown from two different angles through separate snapshots.

Figure 6 (a) Snapshot of β-hairpin formation in all P3Next variant fibrils. (b) The percentage of β-hairpins formed in each fibril. The average percentage of β-hairpins in P3Next-L38M fibril is less than in the fibrils of the other variants. P3Next-WT and L38M aggregated in all seven runs, L38A and V40A did not aggregate in all simulations. The dashed lines and the numbers above them indicate the average percentage of β-hairpins formed by each variant. The figure also displays probability values indicating statistical significance at the top.

Figure 7 (a) A possible mechanism for αSyn-FL-WT aggregation [26]. (b) A possible mechanism for L38M inhibition of αSyn-FL. L38M affects αSyn-FL by reducing β-hairpin formation in P1/P2 region and by inducing antiparallel structures. The colored blocks indicate the regions that are simulated: P1 (red), P2 (green). The rest of the αSyn-FL protein is gray.

1 INTRODUCTION

Amyloid formation by α-synuclein (αSyn), a presynaptic neuronal protein, is associated with several neurodegenerative diseases known as synucleinopathies[1], including Parkinson's disease (PD)[2,3], Parkinson's disease dementia[4], dementia with Lewy bodies[5], and multiple system atrophy[6]. αSyn fibrils are the major constituents of Lewy bodies and Lewy neurites- the cytosolic filamentous inclusions found in neuronal cells of people with synucleinopathies[7]. Since the connection between αSyn aggregation and PD pathology was established in 1997[8], researchers have focused on understanding the aggregation pathways, fibrillar structures, and toxicity of αSyn, with the aim of designing potential therapeutics.

Human αSyn is a 140–amino acid protein that modulates neurotransmitter release[9,10]. Under physiological conditions, it exists as disordered soluble monomers[11,12], membrane-bound (helical) monomers[13,14], and oligomers[15–17]. Full-length αSyn comprises three regions (**Figure 1**): the N-terminal domain (αSyn[1–60]), the central hydrophobic NAC region (αSyn[61–95]), and the C-terminal domain (αSyn[96–140]). Although the NAC region forms the fibril core in all resolved αSyn amyloid structures[18], the N- and C-terminal regions play critical roles in regulating nucleation and aggregation kinetics[19–23].

Multiple lines of evidence implicate the N-terminal region in promoting αSyn self-assembly. Six of the seven familial PD mutations are found within αSyn[46–53][20], and modifications to the imperfect KTKEGV repeats within αSyn[9–30] strongly modulate aggregation[24]. The PreNAC fragment (αSyn[47–56]) forms steric-zipper protofilaments in isolation[25]. The formation of transient β-hairpins in residues αSyn[37-54] is suggested to be an important element in initiating oligomerization by acting as intermolecular binding elements[26]. Multiple experimental approaches that target this same motif have been shown to inhibit αSyn full-

length (αSyn-FL) oligomerization and fibrillation. In one approach, β-wrapin proteins (AS69[27], AS10[28]) bind specifically to the αSyn[37–54] region and stabilize β-hairpin conformations, forming complexes that sequester this aggregation-prone motif and prevent its participation in fibril growth. In another approach, double-cysteine mutants within this region[29,30] stabilize β-hairpins and restrict conformational flexibility, thereby inhibiting fibril elongation of αSyn-FL[29,30].

Two motifs in the N-terminal region of αSyn were identified by Doherty et al.[20] as key modulators of amyloid formation in αSyn-FL: P1 (G_{36}VLYVGS$_{42}$) and P2 (K_{45}EGVVHGVATVAE$_{57}$). Deletion of P1, or of both P1 and P2, or substitution of these regions with alternating glycine–serine sequences, inhibits αSyn aggregation *in vitro*. Deletion of P1 alone prevents amyloid formation at neutral pH, whereas at lower pH deletion of both P1 and P2 is required to achieve the same. Mutational analysis of P1 shows that mutation L38M inhibits the nucleation phase of αSyn-FL amyloid formation but does not prevent fibril elongation from wild-type seeds[31]. More recent research and analyses have reinforced the central role of P1 in oligomer-to-fibril conversion[17] and demonstrated that targeting this region with nanobodies suppresses fibril formation[32].

We investigate the self-assembly mechanisms of the P1 and P2 motifs to understand their roles in αSyn-FL amyloid formation and to clarify how the L38M mutation inhibits fibrillation. The spontaneous aggregation of α-synuclein peptide fragments was studied using discontinuous molecular dynamics (DMD) simulations with the coarse-grained PRIME20 force field, which employs a three-bead backbone with directional hydrogen bonding and residue-specific side-chain interactions to capture secondary structure formation and sequence specificity[33–36]. We focus on a series of fragments of increasing length: P1 (αSyn[36–42]), P2 (αSyn[45–57]), and P3 (αSyn[36–57]), which span P1, P2 and their connecting residues. In addition to L38M, two non-inhibitory

mutations, L38A and V40A, were simulated for comparison. We also studied P3Next (αSyn[27–57]), which extends P3 toward the N-terminus to assess the influence of flanking residues on P1/P2 assembly. We also simulate C1ext (αSyn[14-35]), an extended peptide sequence derived from the C1 motif (αSyn[14–20]) which was selected as a control to mimic the characteristics of the P1 peptide by Doherty et al[20]. They reported that deletion of the C1 motif in full-length αSyn did not produce the same inhibitory effect as deletion of the P1 motif in the same experimental conditions. The C1ext sequence was extended to match the length of P3 to assess whether PRIME20 overpredicts aggregation in αSyn-derived peptides. All peptides are summarized in **Figure 1**.

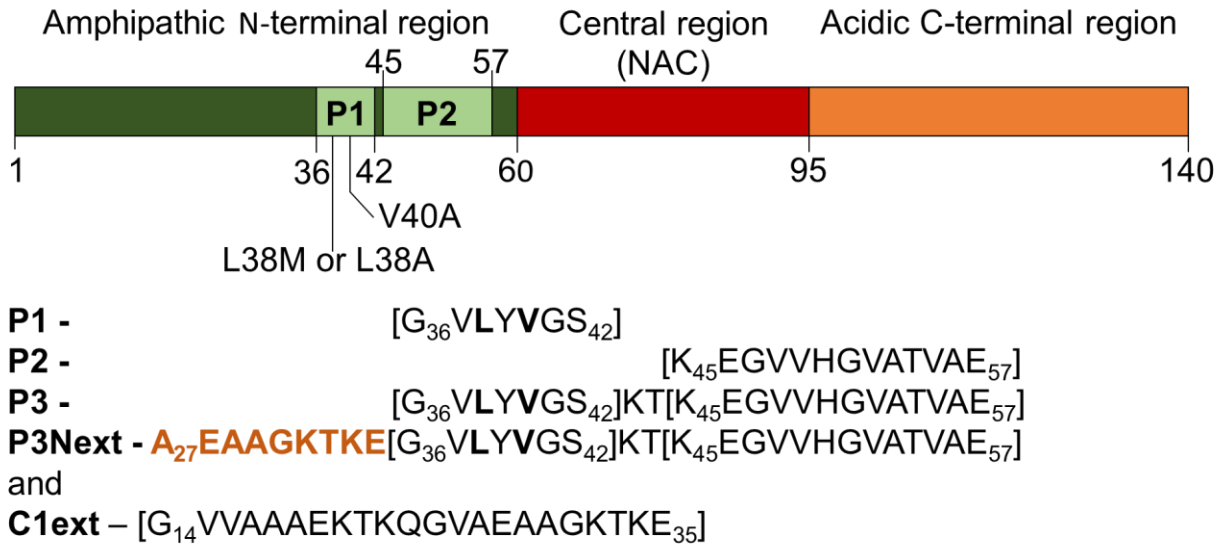

Figure 1 αSyn regions and the peptide fragments that were simulated herein. The amphipathic N-terminal (green) contains residues **αSyn[1-60]**. The central non-amyloid component (NAC) region (red) contains residues **αSyn[61-95]**. The acidic C-terminal region (orange) covers the last 45 residues. P1 and P2 are short motifs in the N-terminal region (light green). The sequences of P1, P2, P3, P3Next, and C1ext are listed. Note the charges on the termini are blocked in the simulation (see Methods).

2 RESULTS AND DISCUSSION

2.1 Wild-type αSyn Fragments Assemble into Fibrillar Structures in All Simulations.

The spontaneous self-assembly of αSyn peptide fragments was investigated using discontinuous molecular dynamics (DMD) simulation with the coarse-grained PRIME20 (Protein Intermediate-Resolution Model) force field. Systems containing 48 P1 peptides or 24 P2, P3, or

P3Next peptides were simulated individually under conditions which allowed the fibrillation process to be completed within a reasonable time frame, resulting in well-ordered secondary structures. Independent simulations were performed for each peptide under each condition explored: three replicas for each P1 variant and for P2, four replicas for each P3 variant, and seven replicas for each P3Next variant. Hence a total of 59 simulations were performed. Simulation concentrations and temperatures are listed in **Table 1**. Each simulation started with a system of peptides in random coil configurations. The systems were equilibrated at fixed temperatures, chosen to have enough energy to escape local minima but not so much as to prevent fibrillation. In the DMD/PRIME20 simulations, all the wild-type fragments (P1, P2, P3, and P3Next) assembled into fibril-like structures with varying types of internal organization. In our simulations, a fragment is considered to be "aggregated" if more than 50% of the runs yield a well-ordered assembly rich in β-sheet structure.

Table 1 Simulation conditions for all sequences.

Sequences	T (K)	Concentration	Number of peptides
P1	310	10mM	48
P2	307	10mM	24
P3	330	10mM	24
P3Next	330	10mM	24
C1ext	330	10mM	24

The simulations of P1-WT show that this sequence favors parallel arrangements of β-strands when forming a β-sheet, which then tends to stack in an antiparallel arrangement. Snapshots of a P1-WT simulation are shown in

Figure 2. At the beginning of the simulation, all P1-WT peptides were in disordered configurations. As time evolved, seven peptides quickly formed a small, disordered cluster (0.24μs) with two parallel layers stacking in antiparallel arrangement. This cluster then grew to form a larger disordered oligomer (0.35μs). The peptides in this oligomer then rearranged

themselves into a five-layer β-sheet-rich conformation (4.08μs). The five-layer structure dissociated and became a smaller four-layer structure (4.18μs). By ~14μs, the P1-WT systems had formed a four-layer fibril with parallel β-sheets stacked in an antiparallel arrangement; this structure persisted until the end of the simulation (~32μs). On average, 90 ± 3% of the residues in the fibril adopted parallel β-strand conformations. Antiparallel strands appear randomly within the P1-WT β-sheets. The time evolution of the percentage of residues in antiparallel β-strands (**Figure S1a**) and potential energy (**Figure S1b**) reveals the coupling between structural organization and energetic stabilization during aggregation. A rapid energy drop within the first few microseconds coincides with a decrease in the number of residues in antiparallel β-strands. After approximately 5 μs, both quantities reached steady values, indicating that the systems had attained stable aggregated states.

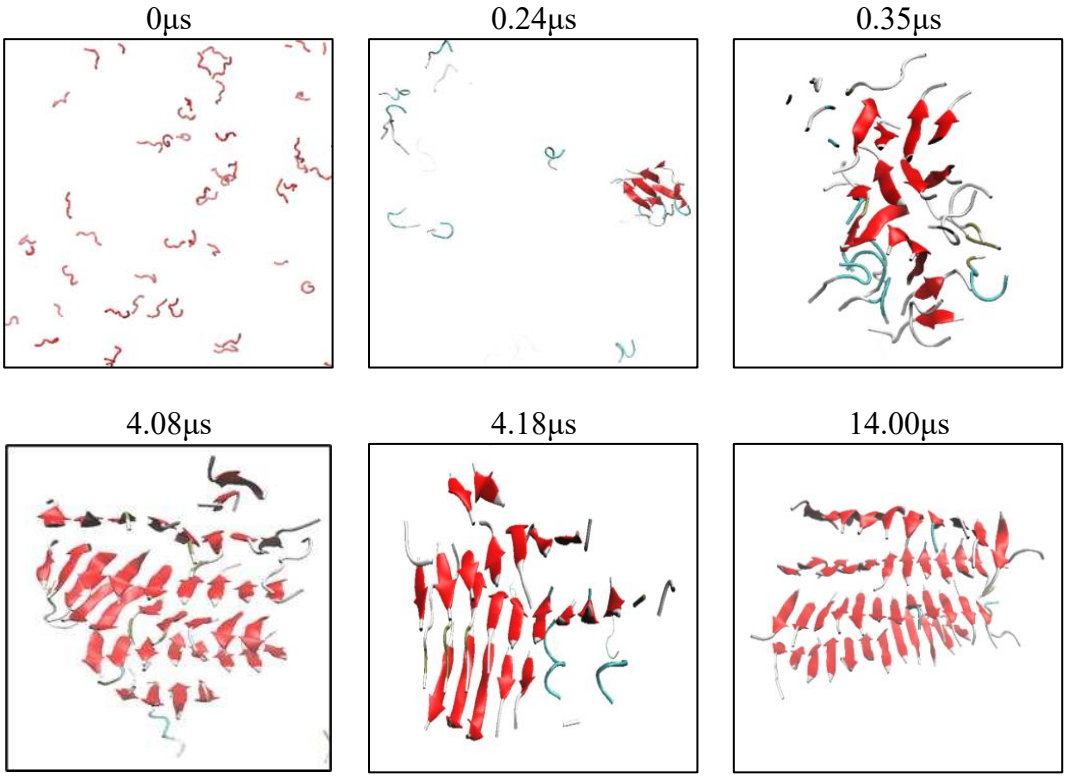

Figure 2 Snapshots at different times during the early stage of fibril formation of P1-WT fragments from one simulation. See **also Supplementary Movie 1**.

In contrast to the P1 peptides, P2 peptides formed single-layer parallel β-sheets that curved into U-shaped or S-shaped fibrils (

Figure 3a; **Supplementary Movies 2 and 3**), which elongated (as opposed to stacking into multilayer assemblies). This curvature arises from the presence of Gly51 near the center of the sequence and the formation of an inward-facing hydrophobic core with charged residues exposed to solvent. Consequently, fragments containing P2 exhibit a high tendency to form bent structures, including β-hairpins. These results are consistent with experimental observations of the PreNAC fragment (αSyn[47–56]), which forms a nanocrystal structure with antiparallel stacked β-sheets. Each β-sheet contained in-register parallel β-strands with a slight bend at G51 on each strand[25]. **Figure S2** presents our simulated structures alongside the PreNAC region of the nanocrystal structure to highlight similarities in key structural features.

The P3-WT peptides formed single-layer β-sheets containing mixtures of parallel and antiparallel strands, the relative proportions of which varied across simulations, indicating that P3-WT can access multiple aggregation pathways. This observation is consistent with the polymorphic behavior observed experimentally in αSyn-FL oligomers[23]. As shown in **Figure S3**, simulation runs in which antiparallel β-sheets remained dominant for extended periods tended to exhibit slower fibril aggregation compared with runs that rapidly transitioned from antiparallel to parallel β-sheet arrangements. The aggregation process of P3-WT Run 3 is recorded in **Supplementary Movie 4**. In contrast to full-length α-synuclein, where intramolecular interactions between the domains[37], intermolecular interactions between proteins[38], and protein-solvent interactions[39] facilitate repeated dissociation and re-association during fibril maturation, our fragment simulations emphasize local aggregation within the P1/P2 motifs. Early in the simulations, peptides undergo frequent association and dissociation events, reflected by large energy fluctuations (

Figure 3c). Once oligomers formed, peptides generally remained stably associated, with fewer pathways for complete dissociation due to the absence of long-range interdomain and solvent-mediated interactions. Local rearrangements and occasional peptide dissociation still occurred to optimize packing, as evidenced by energy fluctuations (

Figure 3c), hydrogen-bond dynamics (**Figure S4**), and **Supplementary Movies**. Consequently, our simulations primarily capture early aggregation kinetics and local structural reorganization of the P1/P2 motifs, rather than long-timescale fibril maturation. To ensure that we do not over-predict aggregation of P3-WT, we also simulated fragment C1ext in the same conditions as for the P3 system. C1ext is an extension of fragment C1 that was predicted to have low amyloid propensity by the Zyggregator method[20]. C1ext did not aggregate in any of our simulations (**Figure S5**), consistent with the prediction.

(a) **P2** fibrils: U-shaped (left) and S-shaped (right)

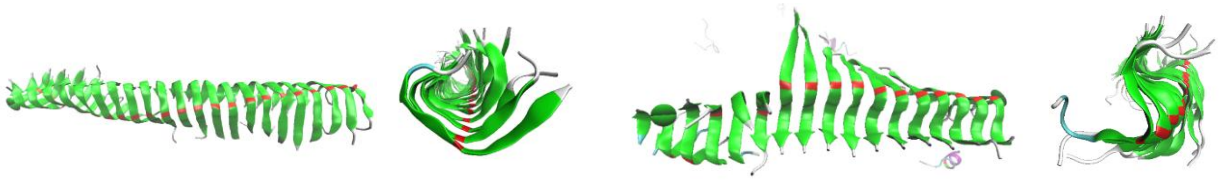

(b) **P3-WT** fibrils

Run 1 Run 2 Run 3 Run 4

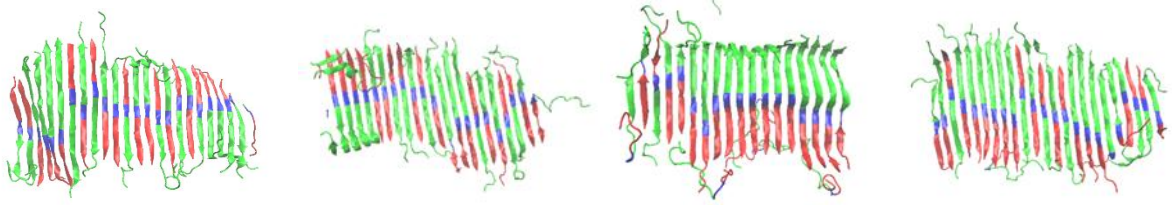

(c)

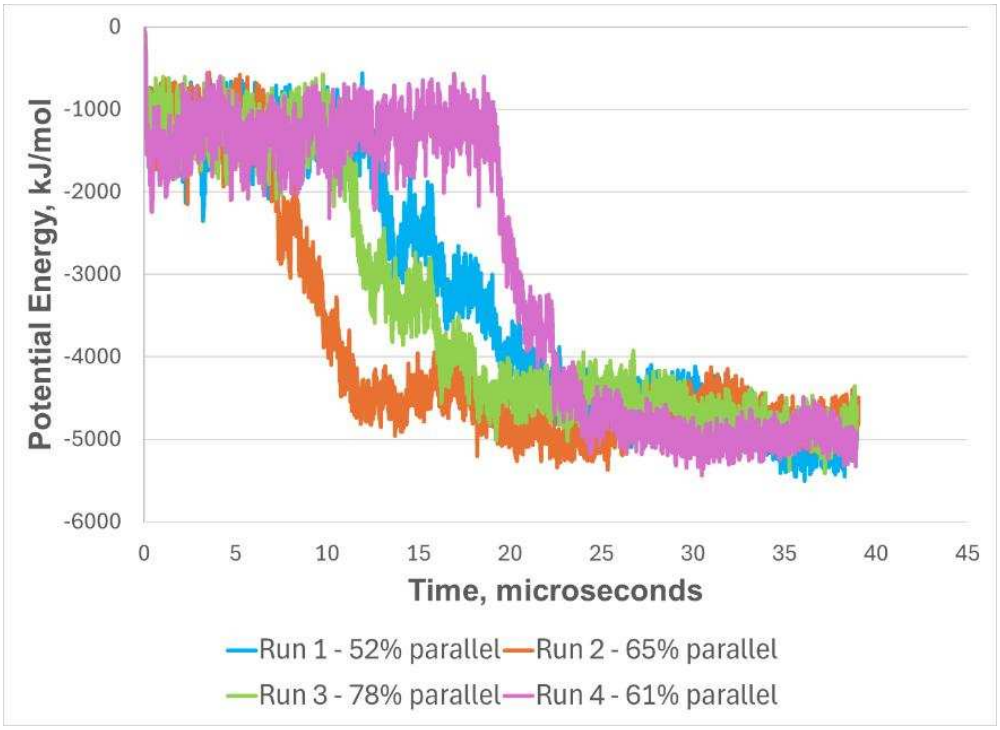

Figure 3 (a) Simulation snapshot of final conformation and schematic representation of U-shaped and S-shaped conformation of P2 fibrils. Red indicates G51 and green shows all other residues. (b) Simulation snapshots of P3 fragments at the end of each run show mixed fibrils with different percentage of parallel residues within the fibrils. As P3 contains both P1 and P2, the color code is used to display the position of P1 (red), P2 (green), and the in-between residues αSyn[43-44] (blue). (c) Total interaction energy vs time for the four runs of P3-WT.

Simulations of P3Next-WT produced β-sheet fibrils with diverse morphologies, all of which contained β-hairpin motifs (

Figure 4a; **Figure S6**). Analysis of β-hairpin counts across seven simulations shows consistent distributions with similar ranges and averages, indicating reproducible behavior rather than kinetic trapping (

Figure 4b). Across all seven simulations, β-hairpins counts are most frequently observed between three and five, with values spanning from near zero to approximately eight, demonstrating broad conformational sampling (

Figure 4c). The average percentage of β-hairpins formed within a single fibril was 23±1%. **Supplementary Movie 5** displays the aggregation process of P3Next-WT in Run 4.

Simulations of various αSyn-WT motifs reveal structural tendencies that favor parallel β-sheets and β-hairpin formation, both of which are associated with enhanced αSyn-FL fibrillation[25,26,40–43]. In the simulations of P3-WT, the fibrils with higher numbers of parallel residues aggregated faster than those with fewer parallel residues, consistent with previous finding that antiparallel transient interactions delay fibrillation[42] and must rearrange to form stable parallel fibrils[43]. Our P3Next-WT (αSyn[27–57]) simulations predicted β-hairpin formation in all simulations. In comparison, Yu et al.[26] found that β-hairpins formed within the P1/P2 region of αSyn-FL act as intermolecular binding elements that promote on-pathway parallel oligomer formation, and that the isolated fragment αSyn[36–55] has an intrinsic propensity to form β-hairpins. However, because our peptide extends further toward the N-terminus than theirs does, the resulting hairpins display differences in geometry and in the positioning of specific residues within the loop, with residue 38 often located at or near the turn. This extension provides an important advantage, as it enables us to capture how single-point mutations at sites such as L38 and V40 alter the local structure — an issue addressed in the following section.

(a)

Run 3

Run 4

(b)

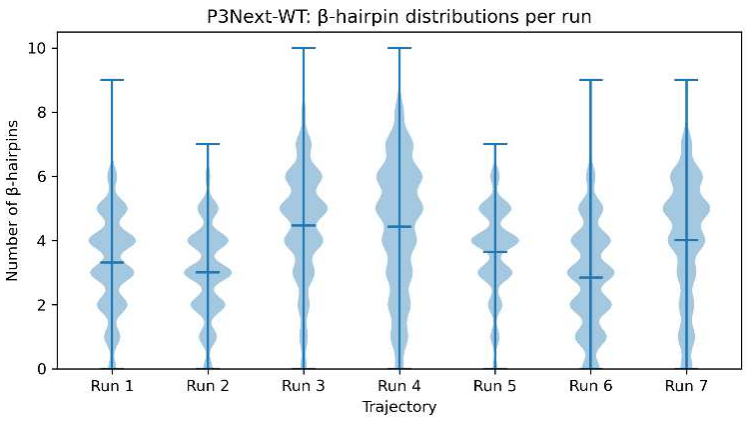

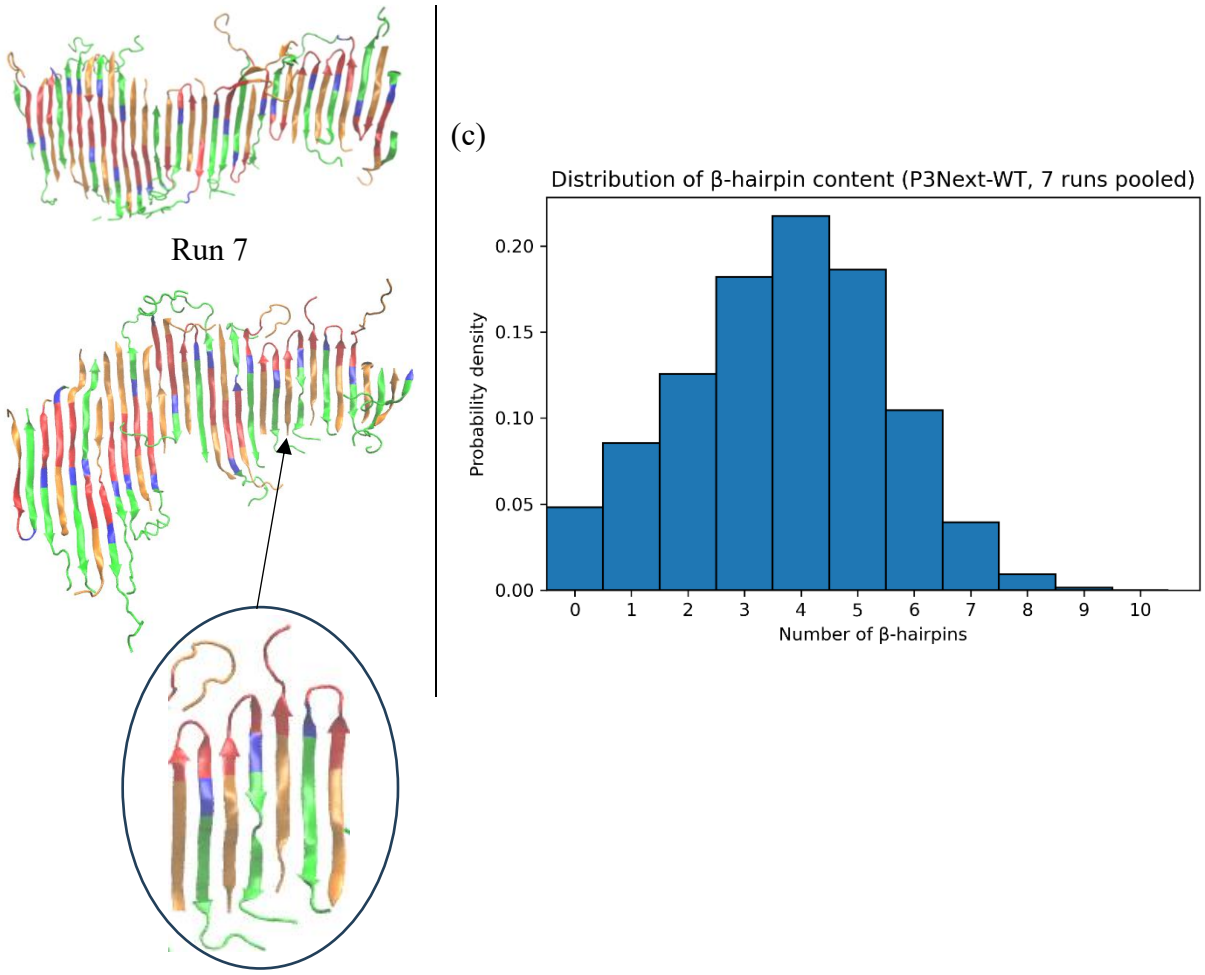

Figure 4 Conformational variability and β-hairpin statistics of P3Next-WT across seven independent simulations. (a) Snapshots at the ends of the simulations of P3Next-WT fragments reveal that the number of β-hairpins varies in the P3Next-WT fibrils. A color code is used to display the position of P1 (red), P2 (green), the in-between residues αSyn[43-44] (blue), and the additional residues in P3Next compared to P3 (orange). Enlarged section from the snapshot of Run 7 shows β-hairpins in the fibril. (b) Distribution of β-hairpin content for each of the seven independent P3Next-WT trajectories, shown as violin plots. Each violin displays the full probability density of β-hairpin counts during a run, with horizontal bars marking the mean and vertical lines indicating extrema. (c) Pooled histogram of β-hairpin content across all frames from all seven WT trajectories shows that distribution is centered around 3–5 β-hairpins.

2.2 Effect of Single-point Mutations L38A, V40A, and L38M on the Self-assembly of Fragments P1, P3, and P3Next.

We next investigated the effect of single point amino acid substitutions, L38A, V40A, and L38M on amyloid formation of αSyn fragments. Previous experiments[31] showed that the substitutions L38A and V40A have no effect on the kinetics of amyloid formation of αSyn-FL, but that L38M inhibits αSyn-FL amyloid assembly (fibrils were not observed at neutral pH over the time course of the experiment). As no experiments have been performed on the equivalent

fragments (substitutions in P1, P2, P3, and P3Next), DMD/PRIME20 simulations were performed on these fragments containing these amino acid changes (**Table 2**) under identical conditions to those used for the wild-type equivalents (**Table 1**). To assess β-sheet formation, we classified each peptide variant as 'aggregates' if β-sheets formed in more than 50% of simulations, 'inconclusive' if 35–50% formed β-sheets, and 'doesn't aggregate' if fewer than 35% of simulations showed any β-sheet formation.

Table 2 PRIME20 simulation results for all αSyn sequences. The term "aggregates" in the table means that β-sheets formed.

Sequences	PRIME20 Simulations
P1-L38A	aggregates
P1-V40A	aggregates
P1-L38M	aggregates
P3-L38A	doesn't aggregate
P3-V40A	inconclusive
P3-L38M	aggregates
P3Next-L38A	aggregates
P3Next-V40A	aggregates
P3Next-L38M	aggregates

Simulations of all P1 variants (WT, L38A, V40A, and L38M) resulted in multilayer fibril formation, but with distinct morphologies (**Figure 5**a and **S7**) and β-strand arrangements (**Figure 5**b). P1-L38A formed prism-like fibrils composed of parallel β-sheets, with reduced antiparallel content (2 ± 0%) relative to WT (10 ± 3%). The irregularity in P1-L38A fibrils resulted from a bend at V40 that created an exposed gap between stacked β-sheets, allowing monomeric P1-L38A to bind at this site and extend into a new β-sheet (**Figure S8**). P1-V40A consistently formed ordered two-layer fibrils with antiparallel stacking between parallel β-sheet layers and an antiparallel content similar to WT (10 ± 4%). In contrast, P1-L38M fibrils contained fewer parallel

strands and exhibited a significantly higher proportion of antiparallel residues (35±2%). These results demonstrate that single-point mutations within P1 alter fibril structures and β-strand arrangements, with L38M uniquely promoting antiparallel arrangements.

(a)

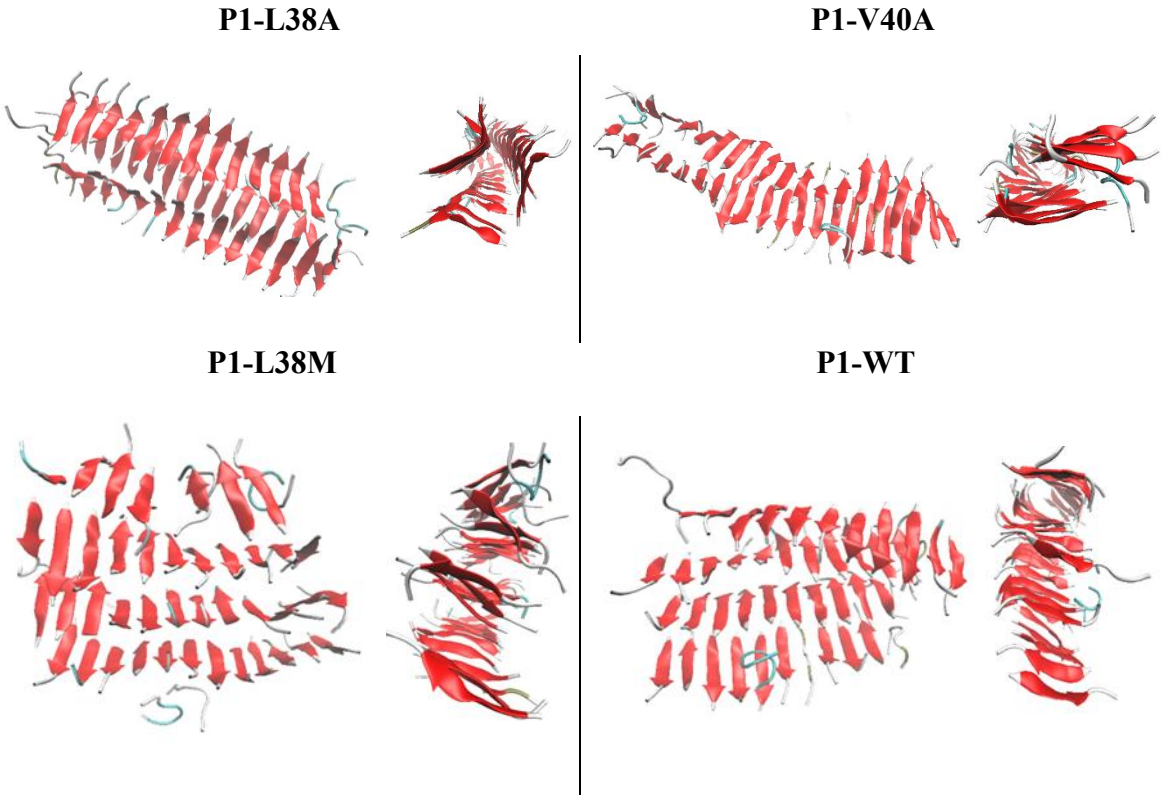

(b)

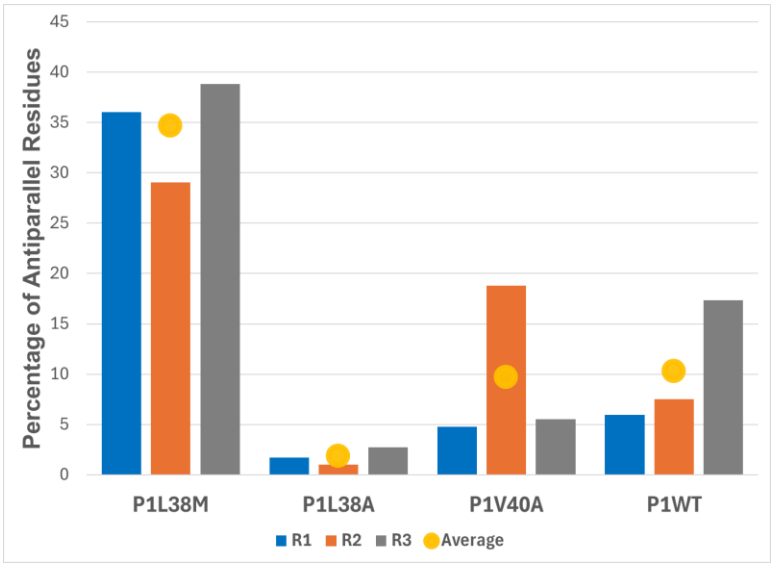

Figure 5 (a) Snapshots of final configurations of P1 peptide simulations with the sequence substitutions L38M, L38A or V40A, as well as the wild-type P1 (P1-WT). Although all four sequences formed multi-layer fibrils, the number of parallel and antiparallel β-strands are different. Each fibril is shown from two different angles through separate snapshots. (b) Average percentage of antiparallel residues within a fibril.

We next examined how sequence alterations affect the self-assembly of P3. In all four simulations, P3-L38M formed single-layer fibrils composed of mixed parallel and anti-parallel strands, similar to P3-WT. In contrast, P3-L38A failed to aggregate in three of four runs, even when simulations were extended to ~39μs (**Figure S9**). The results obtained for P3-V40A were inconclusive as two runs formed mixed fibrils, while all peptides remained as random coils in the other two runs (**Figure S9**). Overall, both L38A and V40A reduced the aggregation propensity of P3 relative to WT. These trends differ from experimental observations for αSyn-FL, where L38A and V40A do not affect fibrillation and L38M inhibits aggregation[31]. In contrast, P3-L38M aggregated consistently in our simulations. This prompted us to consider a peptide that extends beyond P3 toward the N-terminal, P3Next (αSyn[27-57) (**Figure 1**). Note that extension at the C-terminus was not considered as this region incorporates NAC. The increase in peptide length allows assessment of the effect of N-terminal flanking residues. The different behaviors of P3 and P3Next arise from the positions of the mutated residues relative to the β-hairpin–forming region. In the P3 peptide, residues 38 and 40 lie at the N-terminus and cannot participate in the backbone hydrogen-bond network or sidechain packing that stabilizes β-hairpins. Extending the sequence to P3Next places these residues within or adjacent to the turn/strand regions, allowing them to directly influence local backbone geometry, inter-strand packing, and hairpin nucleation.

Simulations of single-point substitutions in P3Next also show that the L38M mutation reduces β-hairpin formation in fibril structures. Final snapshots are shown in **Figure 6**a and **Figure S10-S12**. To quantify the impact of sequence variation, we measured the percentage of β-hairpins in the fibrils formed at the end of each simulation (**Figure 6**b). Although all P3Next-L38M simulations formed fibrils, the average β-hairpin content (16±2%) was lower than that of P3Next-WT (23±1%). The percentage of β-hairpins in fibrils differs significantly between P3Next-L38M

and -WT (p=0.009). In contrast, P3Next-L38A and P3Next-V40A exhibited higher average β-hairpin content (46±8% and 36±6%, respectively), although these differences were not statistically significant relative to that for WT (p = 0.052 and 0.103). To assess whether differences in β-hairpin content among P3Next variants could arise from limited sampling, we performed a statistical power and sample size analysis[44]. For each comparison to P3Next-WT, standardized effect sizes[44] were calculated, and the number of simulations required was estimated (**Table S3**; see **Supplementary Information** for details). Variants with large effects, such as P3Next-L38M and P3Next-L38A, require only 4–5 simulations, indicating that our seven simulations are sufficient. P3Next-V40A, which has only moderate effect, requires 9 simulations. These results indicate that the current sampling adequately captures large mutation-induced differences in β-hairpin formation and that additional simulations are unlikely to alter the qualitative conclusions. The finding that P3Next-L38M has a lower propensity to form β-hairpins compared with P3Next-L38A, -V40A, and -WT is consistent with previous reports suggesting that β-hairpin formation involving P1/P2 could be an important factor in initiating self-assembly of αSyn-FL[26,27].

(a)

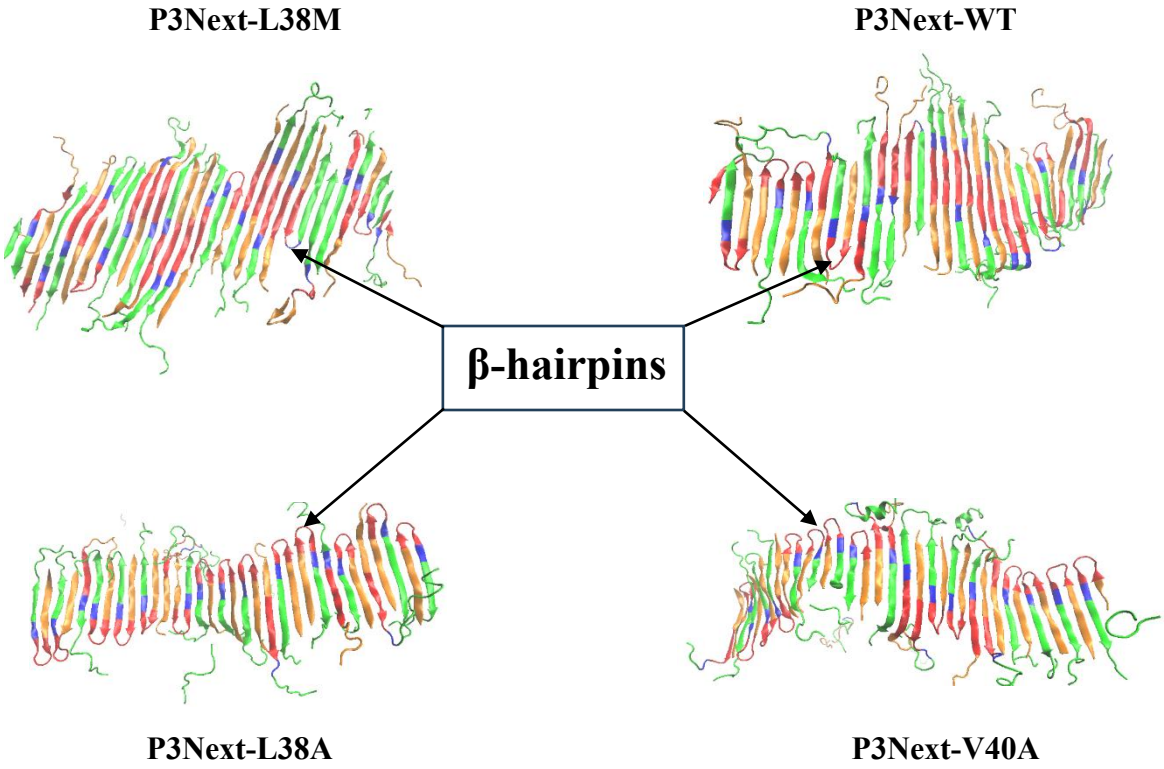

(b)

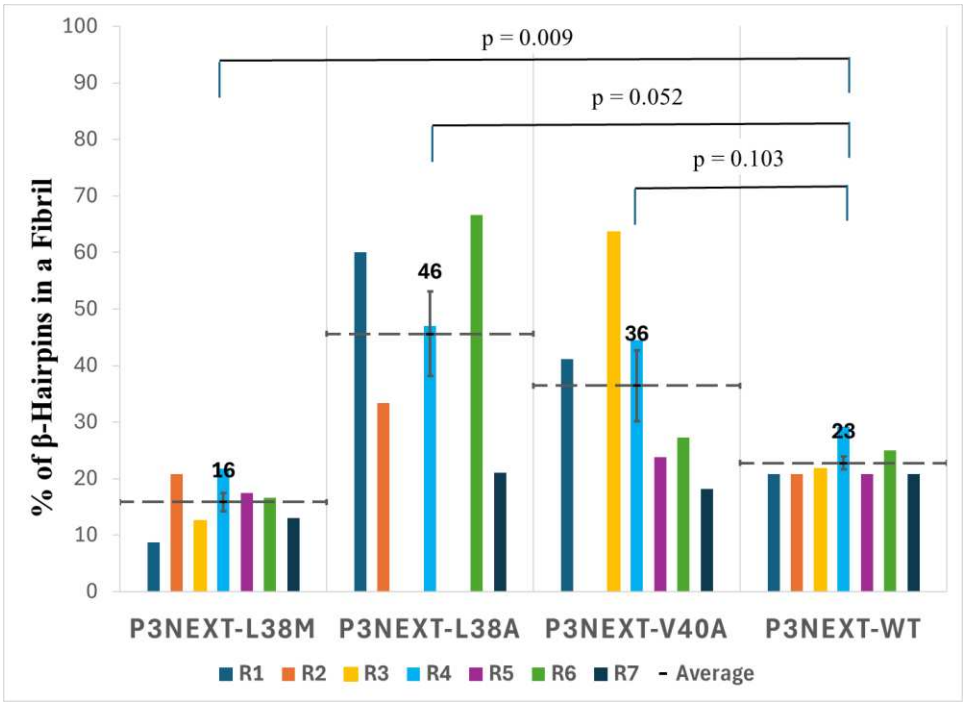

Figure 6 (a) Snapshot of β-hairpin formation in all P3Next variant fibrils. (b) The percentage of β-hairpins formed in each fibril. The average percentage of β-hairpins in P3Next-L38M fibril is less than in the fibrils of the other variants. P3Next-WT and L38M aggregated in all seven runs, L38A and V40A did not aggregate in all simulations. The dashed lines and the numbers above them indicate the average percentage of β-hairpins formed by each variant. The figure also displays probability values indicating statistical significance at the top.

In simulations of L38A and V40A in the P3 and P3Next variants, a small number of simulated systems failed to aggregate, suggesting either kinetic trapping or reduced thermodynamic stability. To distinguish between these possibilities, non-aggregating systems were subjected to a brief temperature-elevation step followed by annealing back to the original simulation temperature, similar to a simulated annealing[45]. Several previously non-aggregating samples reorganized into β-sheets after this perturbation (**Figures S13-14)**, indicating that their initial failure to aggregate arose from kinetic traps. In contrast, a subset of samples remained disordered, suggesting thermodynamic effects. These systems were then simulated at lower temperatures (325 K and 320 K) and results showed enhanced aggregation, with shorter lag times at 320 K (**Figures S15-17)**. Comparison across temperatures shows that the L38A and V40A mutations reduce the effective fibrillization temperature relative to the wild type. These results indicate that the non-aggregating behavior observed for these variants arises from a combination of kinetic trapping and mutation-induced changes in thermodynamic stability.

In addition to the mutations L38M, L38A, and V40A, we simulated two additional variants, Y39A and S42A, which have been reported to increase lag times and to result in the formation of trapped oligomers in α-synuclein fibrillation[17,31]. All the simulation conditions and results are listed on **Table S2**. For P1, both Y39A and S42A exhibited higher antiparallel β-strand content than P1-WT, -L38A, and -V40A, but lower than -L38M, consistent with our overall conclusions. The average percentage of antiparallel content for P1-Y39A and -S42A are 30±2% and 14±1%, respectively (**Figure S19**). However, P3Next-Y39A and -S42A did not show the reduction in β-hairpin formation that is observed in L38M (**Figure S22**). Structural analysis indicates that Y39A, which is located at the β-hairpin turn, tightens the turn and enhances β-hairpin formation (30 ± 3%) compared with L38M (16 ± 2%) and WT (23 ± 1%). S42A, which is positioned on the β-

strand away from the turn, has little effect; therefore, its average β-hairpin content (23 ± 3%) is similar to that of WT. These results highlight the importance of mutation position in modulating β-hairpin structure and aggregation behavior.

Our findings should be interpreted within the scope of the coarse-grained PRIME20 model, which captures the essential physics of peptide aggregation while enabling efficient sampling. PRIME20 was parameterized against 711 PDB protein structures and has successfully reproduced aggregation pathways and fibril morphologies of multiple amyloidogenic peptides in prior studies[36,46–55]. Because PRIME20 does not include explicit solvent or full atomistic interactions, we interpret our results in terms of structural tendencies—such as β-strand registry and β-hairpin formation—rather than absolute thermodynamic stability. To assess the physical stability of representative DMD-predicted fibrils at atomistic resolution, one P1-WT and one P1-L38M fibril were reconstructed to all-atom resolution using PULCHRA (Protein Chain Reconstruction Algorithm)[56] and subjected to explicit-solvent molecular dynamics simulations. Across six independent 500-ns trajectories, the reconstructed fibrils retained their β-sheet architectures (**Figures S23 and S28**), with most peptide chains exhibiting stable Cα RMSD values (<2 Å) (**Figures S24-26 and S29-31**) and no sustained loss of β-sheet content (**Figures S27 and S32**). The absence of significant β-sheet loss of content indicates that the atomistic system preserves the DMD-predicted fibril arrangements.

3 DISCUSSION and CONCLUSIONS

Although αSyn is involved in many neurodegenerative diseases, the mechanism of its amyloid assembly and the role of the N- and C-terminal domains in fibrillation remain unclear. Combining experimental and computational methods can provide insights into molecular interactions that drive or inhibit amyloid formation, including the effects of amino acid

substitutions. For αSyn, oligomerization is thought to be initiated by the formation of β-hairpins within the PreNAC (P2) region[26]. Conversion/growth of the oligomer to the fibril is accelerated by the presence of parallel as opposed to antiparallel conformations[40,42]. We have shown that deleting P1 and P2[20], or mutating Leu 38 to Met (L38M) in P1[31] inhibits αSyn-FL amyloid formation through different effects. In this paper, we use DMD/PRIME20 simulations to provide insight at the molecular level into the impact of these regions on the fibrillation of αSyn fragment variants (P1, P2, P3, P3Next, including both WT and mutated sequences).

Overall, we draw two conclusions from evaluating the fibrillar structures that are formed in the simulations of the peptide variants (WT and mutated). First, WT fragments have a high propensity to form fibrillation-prone structures such as parallel β-sheets and β-hairpins. Second, the mechanism by which L38M prevents the aggregation of αSyn-FL is not by reducing the aggregation propensity of the sequence itself, but by altering its propensity to form the fibrillation-prone structures in the early stages of amyloid formation. The simulations showed that the L38M substitution in the peptide fragment reduces the formation of parallel β-strands for P1 variants and β-hairpins for P3Next variants compared to the WT fragments. In contrast to L38M, the other single-point substitutions, P1-L38A and P1-V40A, increased parallel β-fibril formation for P1 variants and had higher percentages of β-hairpins in their P3Next fibrils. Based on our conclusions and the suggested aggregation mechanism by Yu et al.[26] (**Figure 7**a), we propose two possible inhibition pathways for the L38M point mutation, as illustrated in **Figure 7**b.

The first inhibition pathway shown in Figure 7b suggests that the L38M mutation reduces β-hairpin formation in the P1/P2 region which is proposed to act as an intermolecular binding site during the early stages of oligomerization[26] (**Figure 7**b2.1). This reduction in β-hairpin formation may also hinder the oligomer from adopting conformations necessary for fibril conversion. This

aligns with the recent report by Santos et al.[17], which suggests that the P1/P2 region adopts a folded or partially-folded conformation with specific structural characteristics crucial for oligomer-to-fibril conversion. Although the 38th residue is observed in the hairpins formed by all variants in the simulations, its relative position and the loop length differ between L38M and the other variants. In simulations of P3Next-L38M, residue 38 is typically located within the loop region, occupying either the first or second loop position. In contrast, in P3Next-L38A, V40A or -WT, residue 38 is frequently positioned at the start of the loop or remains part of the β-strand immediately preceding the loop. Although targeting different mutations on the P1/P2 regions from us, Agerschou et al.[29] suggest that the precise position of the β-hairpin is critical to the inhibitory efficiency. An additional observation from our simulations is that the loop in the P3Next-L38M β-hairpin is likely to contain four residues, while the β-hairpins of other variants generally contain three residues. Studies have shown that a shorter loop length stabilizes the β-hairpin structure and accelerates hairpin formation due to a tighter hydrophobic core[57,58]. The preference of L38M for a longer loop length compared to the other variants may reflect methionine's bulkier side chain relative to leucine and alanine, causing it to need additional space within the loop.

The second inhibition pathway suggests that L38M increases antiparallel oligomers (**Figure 7**b2.2), potentially slowing amyloid formation by requiring rearrangement into fibrillation-prone parallel oligomers (**Figure 7**b3.1). Alternatively, it could prevent αSyn-FL fibrillation by stabilizing unproductive oligomers trapped in an antiparallel state (**Figure 7**b3.2). This interpretation is supported by multiple experimental studies showing that antiparallel oligomers are typically associated with off-pathway or prefibrillar species rather than mature αSyn fibrils. Wu and Baum[42] described off-pathway antiparallel oligomer conformations that were incompatible with fibril growth. Celej et al.[19] demonstrated that toxic oligomers can adopt

antiparallel β-sheets which differed from the observed amyloid fibrils. Chen et al.[59] characterized kinetically trapped oligomers that failed to grow to fibrils. Williams et al.[40] reported structural polymorphism among oligomers showing that varying differences in β-strand orientation determine whether an oligomer can convert into a fibril or remain trapped in oligomeric states. In addition, Guzzo et al.[23] reviewed antiparallel-rich intermediates, linking them to off-fibrillation pathways. Taken together, these studies provide precedents for interpreting panel b4 as off-pathway antiparallel oligomers that hinder productive fibril assembly.

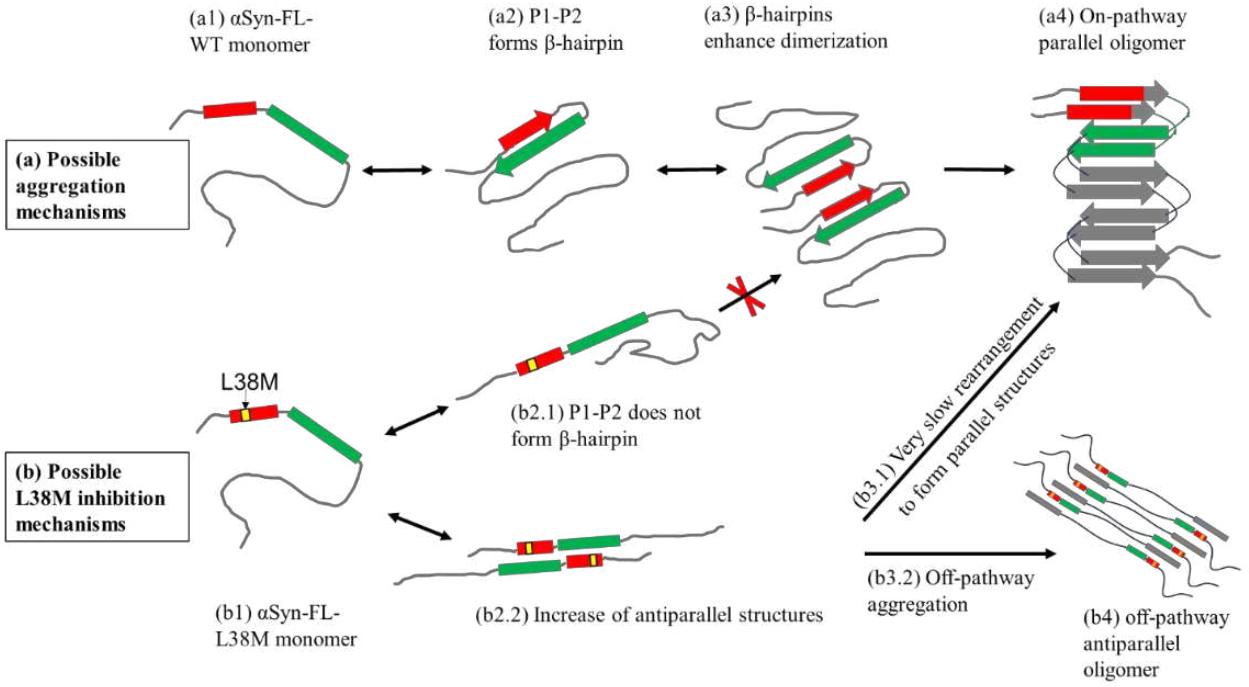

Figure 7 (a) A possible mechanism for αSyn-FL-WT aggregation [26]. (b) A possible mechanism for L38M inhibition of αSyn-FL. L38M affects αSyn-FL by reducing β-hairpin formation in P1/P2 region and by inducing antiparallel structures. The colored blocks indicate the regions that are simulated: P1 (red), P2 (green). The rest of the αSyn-FL protein is gray.

4 MATERIALS AND METHODS

4.1 Discontinuous Molecular Dynamics (DMD) and PRIME20 Force Field

Discontinuous molecular dynamics (DMD) is an event-driven simulation approach that employs discontinuous interaction potentials, enabling efficient sampling at constant temperature

using the Andersen thermostat[60]. PRIME20 is an implicit-solvent, intermediate-resolution coarse-grained protein model developed for use with DMD simulations[33,35,36,61,62]. Each amino acid is represented by four beads, with explicit treatment of backbone geometry, stereochemistry, terminal caps, and directional hydrogen bonding, allowing secondary structure elements such as α-helices and β-sheets to emerge without the use of biasing potentials.[33,36]

PRIME20 was parameterized using a knowledge-based approach against native structures from 711 proteins in the Protein Data Bank and validated by its ability to discriminate native folds from decoys[36]. DMD/PRIME20 has been validated extensively through comparisons with experimental data. Prior studies reproduced fibril formation of Aβ16–22[46], crowding-accelerated aggregation[50], prion nucleation pathways[63], and the thermodynamic phase diagram of Aβ16–22 aggregation[64]. More recent work combined PRIME20 with atomistic MD to investigate the effect of anionic amino acids on co-assembly dynamics and nanofiber structure[48]. The model has also been applied by other groups to study protein folding and aggregation in confinement[65–67], universal aggregation scaling laws[68,69], and single polypeptide chain folding in Monte Carlo simulations[70]. Collectively, these studies demonstrate that PRIME20 reliably captures experimentally relevant aggregation behavior and is broadly applicable to protein folding, self-assembly, and disease-related amyloid systems.

4.2 Relating Reduced Units to Real Units in DMD/PRIME20 Simulations

The PRIME20 model measures time and temperature in terms of reduced units. The real temperature (T, Kelvin) is a linear function of the reduced temperature in PRIME20. The correlation $T^* = (T+115.79)/2288.46$ was obtained by matching the folding temperature of alanine-rich polypeptides in DMD/PRIME20 simulations to experimental values[49]. Conversion to real-time was performed by comparing self-diffusion coefficients of specific peptides in PRIME20

simulations to simulations of the same peptides computed in atomistic simulation at the same concentration. Wang et al. did this conversion using Aβ(16-22) and found that 1 unit of the reduced time in PRIME20 equals approximately 0.96ns in real-time[71].

4.3 Simulation Procedure

All DMD/PRIME20 simulations started from random coil conformations; the peptides aggregated spontaneously to form equilibrium structures[35,46,50]. Simulation temperatures were selected heuristically, consistent with prior PRIME20 studies[35,36,49]. For each wild-type peptide, trial simulations were performed over a range of reduced temperatures (0.175–0.200) to identify conditions that allowed efficient sampling and formation of ordered aggregates within feasible simulation times, while avoiding kinetic trapping in disordered states. All mutant peptides were simulated at the same reduced temperature as their corresponding wild-type sequence to enable direct comparison of mutation effects. Although replica-exchange methods[72] could provide a more systematic approach, they are not readily compatible with event-driven DMD simulations. This pragmatic strategy is consistent with established practice in coarse-grained aggregation studies. Each simulation started at a high temperature of 1028K. Once all the peptides in the simulated system were relaxed into random coils, the temperature was reduced gradually to the desired simulation temperature. The production simulation then proceeded for at least 15μs. For systems that didn't aggregate or hadn't formed a stable structure, simulations were extended to over 35μs. P1, which is only 7 residues long, was simulated in systems with 48 peptide chains (twice the size of other peptide systems) so that the β-sheet alignment and stacking in P1 fibril could be better observed. Details of simulation systems are listed on **Table 1**.

4.4 Quantification of secondary structures

Quantification of parallel and antiparallel residues:

The number of parallel and antiparallel residues in the system was determined using the Define Secondary Structure of Proteins (DSSP) algorithm[73,74]. This method is implemented within our DMD/PRIME20 software suite, which enables identification of hydrogen bonds between backbone atoms. Our algorithm applies the elementary hydrogen-bond patterns for parallel and antiparallel β-bridges, as defined by DSSP, to determine the hydrogen-bonding motif for each residue.

Quantification of β-hairpins:

Secondary structure assignments were obtained using Visual Molecular Dynamics (VMD)[75] with the STRIDE algorithm[76]. These assignments were used to identify β-hairpins and β-strands. A β-hairpin was defined as a strand containing a turn of 2–5 residues, with each turn residue located at least seven residues from either terminus and flanked by at least three consecutive "extended beta" residues on each side. This criterion avoids misidentifying strand termini as turns and ensures the presence of two β-strand segments connected by a turn. A β-strand was defined as a segment containing at least four consecutive "extended beta" residues that participate in a β-sheet. The percentage of β-hairpins was calculated as the total number of β-hairpins divided by the total number of β-strands, multiplied by 100.

Statistical analysis of β-hairpin formation:

Statistical significance of differences in the percentage of β-hairpin formation between each P3Next mutant and WT was evaluated using Welch's t-test[77]. P-values were calculated using the T.TEST function in Microsoft Excel (two-tailed, type = 3), which accounts for unequal variances and unequal sample sizes. A two-tailed test was used to detect differences in either direction relative to the wild-type. Differences were considered statistically significant at $p < 0.05$.

SUPPLEMENTARY MATERIAL

Supplementary material is provided in the file "Supplementary Material for the Publication of in silico peptide self-assembly reveals the importance of N-terminal motifs and the inhibition mechanism of L38M mutation in α-synuclein fibrillation", which includes **Supplementary Figures** showing final snapshots and structural analyses from DMD/PRIME20 simulations of wild-type and mutant α-synuclein fragments. Simulation conditions, peptide sequences, and β-hairpin content for each run are summarized in **Supplementary Table S1 and S2**. Five supplementary movies illustrating representative aggregation processes are available at the provided GitHub links.

ACKNOWLEDGEMENTS

This research was supported by funds from the National Science Foundation (Grants CBET 1835838 and CBET1743432). SMU was funded by Wellcome (215062/Z/18/Z). SER is a Royal Society Professorial Research Fellow (RSRP/R1/211057).

DATA AVAILABILITY

All data supporting the findings of this study are available within the manuscript and the Supplementary Information. Final PDB structures, trajectory and energy profiles, parallel and antiparallel β-sheet analyses, secondary structure profiles obtained using VMD, analysis scripts, Excel spreadsheets, and Supplementary Movies 1–5 are available at: https://github.com/CarolHall-NCSU-CBE/Alpha-Synuclein-Nterminal-Fragments-Simulations-VN.git

The DMD/PRIME20 simulation software is available at:

https://github.com/CarolHall-NCSU-CBE/Serial-DMD-PRIME20

DECLARATION OF COMPETING INTERESTS

The authors declare that they have no known competing interests that could have appeared to influence the work reported in this paper.

REFERENCES

1. Bisi, N. *et al.* α-Synuclein: An All-Inclusive Trip Around its Structure, Influencing Factors and Applied Techniques. *Front. Chem.* **9**, 666585 (2021).
2. Parkinson, J. An Essay on the Shaking Palsy. *JNP* **14**, 223–236 (2002).
3. Goetz, C. G. The history of Parkinson's disease: early clinical descriptions and neurological therapies. *Cold Spring Harb Perspect Med* **1**, a008862 (2011).
4. Emre, M. *et al.* Clinical diagnostic criteria for dementia associated with Parkinson's disease. *Movement Disorders* **22**, 1689–1707 (2007).
5. McKeith, I. G. *et al.* Diagnosis and management of dementia with Lewy bodies: Third report of the DLB consortium. *Neurology* **65**, 1863–1872 (2005).
6. Grazia Spillantini, M. *et al.* Filamentous α-synuclein inclusions link multiple system atrophy with Parkinson's disease and dementia with Lewy bodies. *Neuroscience Letters* **251**, 205–208 (1998).
7. Spillantini, M. G., Crowther, R. A., Jakes, R., Hasegawa, M. & Goedert, M. α-Synuclein in filamentous inclusions of Lewy bodies from Parkinson's disease and dementia with Lewy bodies. *Proc. Natl. Acad. Sci. U.S.A.* **95**, 6469–6473 (1998).
8. Spillantini, M. G. *et al.* α-Synuclein in Lewy bodies. *Nature* **388**, 839–840 (1997).
9. Cabin, D. E. *et al.* Synaptic Vesicle Depletion Correlates with Attenuated Synaptic Responses to Prolonged Repetitive Stimulation in Mice Lacking α-Synuclein. *J. Neurosci.* **22**, 8797–8807 (2002).
10. Murphy, D. D., Rueter, S. M., Trojanowski, J. Q. & Lee, V. M.-Y. Synucleins Are Developmentally Expressed, and α-Synuclein Regulates the Size of the Presynaptic Vesicular Pool in Primary Hippocampal Neurons. *J. Neurosci.* **20**, 3214–3220 (2000).

11. Fauvet, B. *et al.* α-Synuclein in Central Nervous System and from Erythrocytes, Mammalian Cells, and Escherichia coli Exists Predominantly as Disordered Monomer. *Journal of Biological Chemistry* **287**, 15345–15364 (2012).
12. Burré, J. *et al.* Properties of native brain α-synuclein. *Nature* **498**, E4–E6 (2013).
13. Eliezer, D., Kutluay, E., Bussell, R. & Browne, G. Conformational properties of α-synuclein in its free and lipid-associated states 1 1Edited by P. E. Wright. *Journal of Molecular Biology* **307**, 1061–1073 (2001).
14. Ulmer, T. S., Bax, A., Cole, N. B. & Nussbaum, R. L. Structure and Dynamics of Micelle-bound Human α-Synuclein. *Journal of Biological Chemistry* **280**, 9595–9603 (2005).
15. Lorenzen, N. *et al.* The Role of Stable α-Synuclein Oligomers in the Molecular Events Underlying Amyloid Formation. *J. Am. Chem. Soc.* **136**, 3859–3868 (2014).
16. Dear, A. J. *et al.* Kinetic diversity of amyloid oligomers. *Proc. Natl. Acad. Sci. U.S.A.* **117**, 12087–12094 (2020).
17. Santos, J. *et al.* A Targetable N-Terminal Motif Orchestrates α-Synuclein Oligomer-to-Fibril Conversion. *J. Am. Chem. Soc.* **146**, 12702–12711 (2024).
18. Sawaya, M. R., Hughes, M. P., Rodriguez, J. A., Riek, R. & Eisenberg, D. S. The expanding amyloid family: Structure, stability, function, and pathogenesis. *Cell* **184**, 4857–4873 (2021).
19. Celej, M. S. *et al.* Toxic prefibrillar α-synuclein amyloid oligomers adopt a distinctive antiparallel β-sheet structure. *Biochemical Journal* **443**, 719–726 (2012).
20. Doherty, C. P. A. *et al.* A short motif in the N-terminal region of α-synuclein is critical for both aggregation and function. *Nat Struct Mol Biol* **27**, 249–259 (2020).
21. Sorrentino, Z. A. & Giasson, B. I. The emerging role of α-synuclein truncation in aggregation and disease. *Journal of Biological Chemistry* **295**, 10224–10244 (2020).

22. Farzadfard, A. *et al.* The C-terminal tail of α-synuclein protects against aggregate replication but is critical for oligomerization. *Commun Biol* **5**, 123 (2022).
23. Guzzo, A. *et al.* Wild-Type α-Synuclein and Variants Occur in Different Disordered Dimers and Pre-Fibrillar Conformations in Early Stage of Aggregation. *Front. Mol. Biosci.* **9**, 910104 (2022).
24. Kessler, J. C., Rochet, J.-C. & Lansbury, P. T. The N-Terminal Repeat Domain of α-Synuclein Inhibits β-Sheet and Amyloid Fibril Formation. *Biochemistry* **42**, 672–678 (2003).
25. Rodriguez, J. A. *et al.* Structure of the toxic core of α-synuclein from invisible crystals. *Nature* **525**, 486–490 (2015).
26. Yu, H., Han, W., Ma, W. & Schulten, K. Transient β -hairpin formation in α -synuclein monomer revealed by coarse-grained molecular dynamics simulation. *The Journal of Chemical Physics* **143**, 243142 (2015).
27. Mirecka, E. A. *et al.* Sequestration of a β-Hairpin for Control of α-Synuclein Aggregation. *Angew Chem Int Ed* **53**, 4227–4230 (2014).
28. Orr, A. A., Wördehoff, M. M., Hoyer, W. & Tamamis, P. Uncovering the Binding and Specificity of β-Wrapins for Amyloid-β and α-Synuclein. *J. Phys. Chem. B* **120**, 12781–12794 (2016).
29. Agerschou, E. D., Borgmann, V., Wördehoff, M. M. & Hoyer, W. Inhibitor and substrate cooperate to inhibit amyloid fibril elongation of α-synuclein. *Chem. Sci.* **11**, 11331–11337 (2020).
30. Shaykhalishahi, H. *et al.* Contact between the β1 and β2 Segments of α-Synuclein that Inhibits Amyloid Formation. *Angew Chem Int Ed* **54**, 8837–8840 (2015).

31. Ulamec, S. M. *et al.* Single residue modulators of amyloid formation in the N-terminal P1-region of α-synuclein. *Nat Commun* **13**, 4986 (2022).
32. Gialama, D., Vadukul, D. M., Thrush, R. J., Radford, S. E. & Aprile, F. A. A Potent Sybody Selectively Inhibits α-Synuclein Amyloid Formation by Binding to the P1 Region. *J. Med. Chem.* **67**, 9857–9868 (2024).
33. Voegler-Smith, A. & Hall, C. K. α-Helix formation: Discontinuous molecular dynamics on an intermediate-resolution protein model. *Proteins* **44**, 344–360 (2001).
34. Marchut, A. J. & Hall, C. K. Spontaneous formation of annular structures observed in molecular dynamics simulations of polyglutamine peptides. *Computational Biology and Chemistry* **30**, 215–218 (2006).
35. Nguyen, H. D. & Hall, C. K. Molecular dynamics simulations of spontaneous fibril formation by random-coil peptides. *Proc. Natl. Acad. Sci. U.S.A.* **101**, 16180–16185 (2004).
36. Cheon, M., Chang, I. & Hall, C. K. Extending the PRIME model for protein aggregation to all 20 amino acids. *Proteins* **78**, 2950–2960 (2010).
37. Dedmon, M. M., Lindorff-Larsen, K., Christodoulou, J., Vendruscolo, M. & Dobson, C. M. Mapping Long-Range Interactions in α-Synuclein using Spin-Label NMR and Ensemble Molecular Dynamics Simulations. *J. Am. Chem. Soc.* **127**, 476–477 (2005).
38. Carulla, N. *et al.* Molecular recycling within amyloid fibrils. *Nature* **436**, 554–558 (2005).
39. Becker, S., Giller, K., Sieme, D. & Rezaei-Ghaleh, N. Maturation of amyloid β fibrils alters their molecular stability. *Phys. Chem. Chem. Phys.* **25**, 15099–15103 (2023).
40. Williams, J. K., Yang, X. & Baum, J. Interactions between the Intrinsically Disordered Proteins β-Synuclein and α-Synuclein. *Proteomics* **18**, 1800109 (2018).

41. Tuttle, M. D. *et al.* Solid-state NMR structure of a pathogenic fibril of full-length human α-synuclein. *Nat Struct Mol Biol* **23**, 409–415 (2016).
42. Wu, K.-P. & Baum, J. Detection of Transient Interchain Interactions in the Intrinsically Disordered Protein α-Synuclein by NMR Paramagnetic Relaxation Enhancement. *J. Am. Chem. Soc.* **132**, 5546–5547 (2010).
43. Zhou, L. & Kurouski, D. Structural Characterization of Individual α-Synuclein Oligomers Formed at Different Stages of Protein Aggregation by Atomic Force Microscopy-Infrared Spectroscopy. *Anal. Chem.* **92**, 6806–6810 (2020).
44. Cohen, J. *Statistical Power Analysis for the Behavioral Sciences*. (Routledge, 2013). doi:10.4324/9780203771587.
45. Kirkpatrick, S., Gelatt, C. D. & Vecchi, M. P. Optimization by Simulated Annealing. *Science* **220**, 671–680 (1983).
46. Cheon, M., Chang, I. & Hall, C. K. Spontaneous Formation of Twisted Aβ16-22 Fibrils in Large-Scale Molecular-Dynamics Simulations. *Biophysical Journal* **101**, 2493–2501 (2011).
47. Wang, Y. & Hall, C. K. Seeding and cross-seeding fibrillation of N-terminal prion protein peptides PrP(120–144). *Protein Science* **27**, 1304–1313 (2018).
48. Dong, X. Y., Liu, R., Seroski, D. T., Hudalla, G. A. & Hall, C. K. Programming co-assembled peptide nanofiber morphology via anionic amino acid type: Insights from molecular dynamics simulations. *PLoS Comput Biol* **19**, e1011685 (2023).
49. Wang, Y., Shao, Q. & Hall, C. K. N-terminal Prion Protein Peptides (PrP(120–144)) Form Parallel In-register β-Sheets via Multiple Nucleation-dependent Pathways. *Journal of Biological Chemistry* **291**, 22093–22105 (2016).

50. Latshaw, D. C., Cheon, M. & Hall, C. K. Effects of Macromolecular Crowding on Amyloid Beta (16–22) Aggregation Using Coarse-Grained Simulations. *J. Phys. Chem. B* **118**, 13513–13526 (2014).
51. Cheon, M., Chang, I. & Hall, C. K. Influence of temperature on formation of perfect tau fragment fibrils using PRIME20/DMD simulations. *Protein Science* **21**, 1514–1527 (2012).
52. Latshaw, D. C. & Hall, C. K. Effects of Hydrophobic Macromolecular Crowders on Amyloid β (16–22) Aggregation. *Biophysical Journal* **109**, 124–134 (2015).
53. Wagoner, V. A., Cheon, M., Chang, I. & Hall, C. K. Fibrillization Propensity for Short Designed Hexapeptides Predicted by Computer Simulation. *Journal of Molecular Biology* **416**, 598–609 (2012).
54. Wagoner, V. A., Cheon, M., Chang, I. & Hall, C. K. Impact of sequence on the molecular assembly of short amyloid peptides. *Proteins* **82**, 1469–1483 (2014).
55. Cheon, M., Hall, C. K. & Chang, I. Structural Conversion of Aβ17–42 Peptides from Disordered Oligomers to U-Shape Protofilaments via Multiple Kinetic Pathways. *PLoS Comput Biol* **11**, e1004258 (2015).
56. Rotkiewicz, P. & Skolnick, J. Fast procedure for reconstruction of full-atom protein models from reduced representations. *J Comput Chem* **29**, 1460–1465 (2008).
57. Andersen, N. H. *et al.* Minimization and Optimization of Designed β-Hairpin Folds. *J. Am. Chem. Soc.* **128**, 6101–6110 (2006).
58. Colombo, G., De Mori, G. M. S. & Roccatano, D. Interplay between hydrophobic cluster and loop propensity in β-hairpin formation: A mechanistic study. *Protein Science* **12**, 538–550 (2003).

59. Chen, S. W. *et al.* Structural characterization of toxic oligomers that are kinetically trapped during α-synuclein fibril formation. *Proc. Natl. Acad. Sci. U.S.A.* **112**, (2015).

60. Andersen, H. C. Molecular dynamics simulations at constant pressure and/or temperature. *The Journal of Chemical Physics* **72**, 2384–2393 (1980).

61. Voegler-Smith, A. & Hall, C. K. Assembly of a tetrameric α-helical bundle: Computer simulations on an intermediate-resolution protein model. *Proteins* **44**, 376–391 (2001).

62. Nguyen, H. D., Marchut, A. J. & Hall, C. K. Solvent effects on the conformational transition of a model polyalanine peptide. *Protein Science* **13**, 2909–2924 (2004).

63. Wang, Y., Latshaw, D. C. & Hall, C. K. Aggregation of Aβ(17–36) in the Presence of Naturally Occurring Phenolic Inhibitors Using Coarse-Grained Simulations. *Journal of Molecular Biology* **429**, 3893–3908 (2017).

64. Wang, Y. *et al.* Thermodynamic phase diagram of amyloid-β (16–22) peptide. *Proc. Natl. Acad. Sci. U.S.A.* **116**, 2091–2096 (2019).

65. Javidpour, L., Tabar, M. R. R. & Sahimi, M. Molecular simulation of protein dynamics in nanopores. I. Stability and folding. *The Journal of Chemical Physics* **128**, 115105 (2008).

66. Javidpour, L., Tabar, M. R. R. & Sahimi, M. Molecular simulation of protein dynamics in nanopores. II. Diffusion. *The Journal of Chemical Physics* **130**, 085105 (2009).

67. Javidpour, L. & Sahimi, M. Confinement in nanopores can destabilize α-helix folding proteins and stabilize the β structures. *The Journal of Chemical Physics* **135**, 125101 (2011).

68. Zheng, S., Javidpour, L., Shing, K. S. & Sahimi, M. Dynamics of proteins aggregation. I. Universal scaling in unbounded media. *The Journal of Chemical Physics* **145**, 134306 (2016).

69. Zheng, S., Shing, K. S. & Sahimi, M. Dynamics of proteins aggregation. II. Dynamic scaling in confined media. *The Journal of Chemical Physics* **148**, 104305 (2018).

70. Böker, A. & Paul, W. Thermodynamics and Conformations of Single Polyalanine, Polyserine, and Polyglutamine Chains within the PRIME20 Model. *J. Phys. Chem. B* **126**, 7286–7297 (2022).

71. Wang, Y., Shao, Q. & Hall, C. K. N-terminal prion protein peptides (PrP(120–144)) form parallel in-register β-sheets via multiple nucleation-dependent pathways. *Journal of Biological Chemistry* **292**, 20655 (2017).

72. Sugita, Y. & Okamoto, Y. Replica-exchange molecular dynamics method for protein folding. *Chemical Physics Letters* **314**, 141–151 (1999).

73. Kabsch, W. & Sander, C. Dictionary of protein secondary structure: Pattern recognition of hydrogen-bonded and geometrical features. *Biopolymers* **22**, 2577–2637 (1983).

74. Gorelov, S., Titov, A., Tolicheva, O., Konevega, A. & Shvetsov, A. DSSP in GROMACS: Tool for Defining Secondary Structures of Proteins in Trajectories. *J. Chem. Inf. Model.* **64**, 3593–3598 (2024).

75. Humphrey, W., Dalke, A. & Schulten, K. VMD: Visual molecular dynamics. *Journal of Molecular Graphics* **14**, 33–38 (1996).

76. Frishman, D. & Argos, P. Knowledge-based protein secondary structure assignment. *Proteins* **23**, 566–579 (1995).

77. Welch, B. L. ON THE COMPARISON OF SEVERAL MEAN VALUES: AN ALTERNATIVE APPROACH. *Biometrika* **38**, 330–336 (1951).